Preparation, Transport Properties, and Structure Analysis by Resonant X-ray Scattering of the Type I Clathrate $Cs_8Cd_4Sn_{42}$

A. P. Wilkinson,*,† C. Lind,† R. A. Young,‡ S. D. Shastri,§ P. L. Lee,§ and G. S. Nolas⊥

School of Chemistry and Biochemistry, Georgia Institute of Technology, Atlanta, Georgia 30332-0400; School of Physics, Georgia Institute of Technology, Atlanta, Georgia 30332-0430; SRI-CAT, Advanced Photon Source, Argonne National Laboratory, Illinois 60439-4803; and Department of Physics, University of South Florida, Tampa, Florida 33620-5700

Received September 12, 2001. Revised Manuscript Received January 8, 2002

Structural and transport properties of $Cs_8Cd_4Sn_{42}$ are reported. $Cs_8Cd_4Sn_{42}$ has a thermal conductivity that is unusually low for a crystalline solid (1 W m^{-1} K^{-1} at room temperature). This low lattice thermal conductivity is associated with the rattling of cesium in the tetrakaidecahedral cavities, as indicated by the large atomic displacement parameters of Cs in the tretrakaidecahedra. Resonant X-ray powder diffraction measurements indicate that all of the cadmium is located on one of three inequivalent framework sites. There is no evidence for any framework vacancies in the material.

Introduction

Clathrates with frameworks built up from group 14 atoms have been known since the work of Cros et al. on Na_8Si_{46} and Na_xSi_{136}.[1,2] These materials have crystal structures closely related to those of type I and type II gas hydrates such as $(Cl_2)_8(H_2O)_{46}$ and $(CO_2)_{24}(H_2O)_{136}$.[3] Several different compositions with these two structures have been prepared,[4,5] as they are of fundamental interest from the perspective of both bonding and their physical properties. Superconductivity has been reported in compounds such as $(Na,Ba)_xSi_{46}$[6] and $Ba_8Ga_{16}Ge_{30}$.[7] The possibility of large band gaps[8] in some materials has attracted interest from the perspective of optical applications. The very low thermal conductivity found in some materials has also aroused interest.[9−11] The type I clathrates $Sr_8Ga_{16}Ge_{30}$ and $Eu_8Ga_{16}Ge_{30}$ display glasslike thermal conductivities along with good charge carrier mobility and can be considered as phonon glass−electron crystals.[10] This combination of properties makes them good candidates for thermoelectric applications.[11−13]

Most type I clathrates are Zintl phases.[14] As alkali, alkaline earth, or rare earth atoms are introduced into the cages of the clathrate structure, the framework composition is modified to maintain the correct valence electron count. This can be done either by replacing some of the group 14 atoms in the framework with group 12 or 13 atoms or by generating framework vacancies. In tin framework materials, both mechanisms have been observed. For example, Zn substitution in $Cs_8Zn_4Sn_{42}$[15] and vacancy formation in both Rb_8Sn_{44}[16] and Cs_8Sn_{44}[17] achieve the required electron counts. Typically, in type I clathrates, vacancies or group 12/13 atoms that are present in order to maintain the correct valence electron count are not randomly distributed over the three crystallographically distinct framework sites (see Figure 1),[18−24] although a random distribution has been re-

† School of Chemistry and Biochemistry, Georgia Institute of Technology.
‡ School of Physics, Georgia Institute of Technology.
§ Argonne National Laboratory.
⊥ University of South Florida.

(1) Cros, C.; Pouchard, M.; Hagenmuller, P. *C. R. Acad. Sci. Paris* **1965**, *260*, 4764−4767.
(2) Kasper, J. S.; Hagenmuller, P.; Pouchard, M.; Cros, C. *Science* **1965**, *150*, 1713−1714.
(3) Jeffrey, G. A. In *Inclusion Compounds*; Atwood, J. L., Davies, J. E. D., MacNicol, D. D., Eds.; Academic Press: New York, 1984; Vol. 1, pp 135−190.
(4) Eisenmann, B.; Schafer, H.; Zagler, R. *J. Less-Common Met.* **1986**, *118*, 43−55.
(5) Bobev, S.; Sevov, S. C. *J. Solid State Chem.* **2000**, *153*, 92−105.
(6) Kawaji, H.; Horie, H.-O.; Yamanaka, S.; Ishikawa, M. *Phys. Rev. Lett.* **1995**, *74*, 1427−1429.
(7) Bryan, J. D.; Srdanov, V. I.; Stucky, G. D.; Schmidt, D. *Phys. Rev. B* **1999**, *60*, 3064−3067.
(8) Adams, G. B.; O'Keefe, M.; Demkov, A. A.; Sankey, O. F.; Huang, Y.-M. *Phys. Rev. B* **1994**, *49*, 8048−8053.
(9) Keppens, V.; Sales, B. C.; Mandrus, D.; Chakoumakos, B. C. *Philos. Mag. Lett.* **2000**, *80*, 807−812.
(10) Cohn, J. L.; Nolas, G. S.; Fessatidis, V.; Metcalf, T. H.; Slack, G. A. *Phys. Rev. Lett.* **1999**, *82*, 779−782.
(11) Nolas, G. S.; Cohn, J. L.; Slack, G. A.; Schujman, S. B. *Appl. Phys. Lett.* **1998**, *73*, 178−180.
(12) Nolas, G. S.; Weakley, T. J. R.; Cohn, J. L.; Sharma, R. *Phys. Rev. B* **2000**, *61*, 3845.
(13) Nolas, G. S.; Slack, G. A.; Schujman, S. B. In *Recent Trends in Thermoelectric Materials Research I*; Tritt, T. M., Ed.; Academic Press: San Diego, 2001; Vol. 69, pp 255−300.
(14) Kauzlarich, S. M. *Chemistry, Structure, and Bonding of Zintl Phases and Ions*; VCH: New York, 1996.
(15) Nolas, G. S.; Weakley, T. J. R.; Cohn, J. L. *Chem. Mater.* **1999**, *11*, 2470−2473.
(16) Zhao, J.-T.; Corbett, J. D. *Inorg. Chem.* **1994**, *33*, 5721−5726.
(17) Nolas, G. S.; Chakoumakos, B. C.; Mahieu, B.; Long, G. J.; Weakley, T. J. R. *Chem. Mater.* **2000**, *12*, 1947−1953.
(18) Kroner, R.; Peters, K.; von Schnering, H. G. *Z. Kristallogr.—New Cryst. Struct.* **1998**, *213*, 671−672.
(19) von Schnering, H. G.; Kroner, R.; Menke, H.; Peters, K. *Z. Kristallogr.—New Cryst. Struct.* **1998**, *213*, 677−678.
(20) von Schnering, H. G.; Menke, H.; Kroner, R.; Peters, E.-M.; Peters, K. *Z. Kristallogr.—New Cryst. Struct.* **1998**, *213*, 673−674.

10.1021/cm0107880 CCC: $22.00
Published on Web 02/28/2002

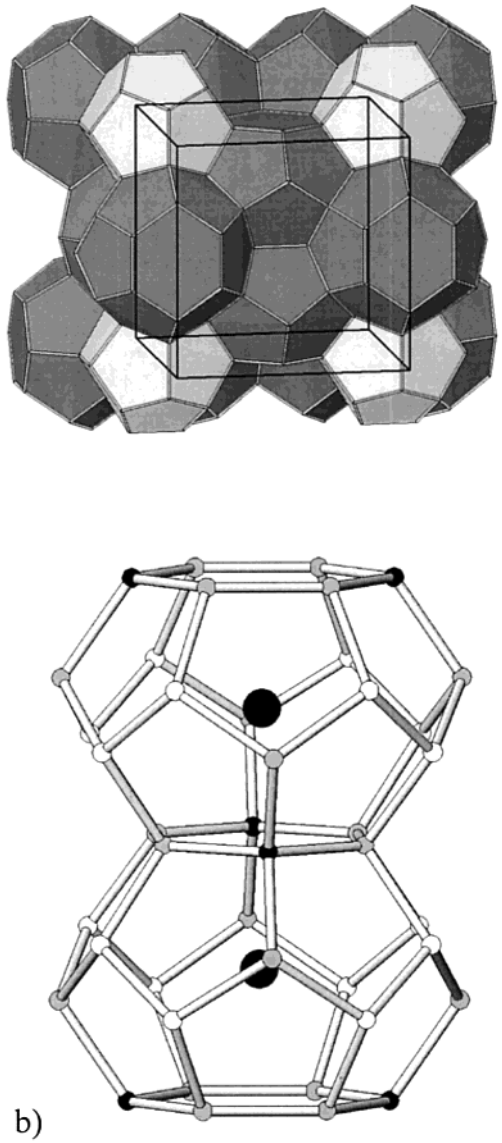

Figure 1. (a) Framework structure of a type I clathrate consists of face sharing dodecahedra (light gray) and tetrakaidecahedra (dark gray). (b) There are three crystallographically distinct sites in the framework. The 6c, 16i, and 24k positions are indicated as black, white, and gray small spheres, respectively.

ported for $Sr_8Ga_{16}Ge_{30}$.[25] Electronic structure calculations suggest that the distribution of the framework components can have a very significant effect on the Seebeck coefficients for these materials.[26] Consequently, the determination of these distributions and how they depend on sample preparation may play an important role in optimizing the thermoelectric properties of type I clathrates.

Nearly all of the experimental work examining the distribution of substituting atoms in clathrate frameworks has focused on materials where there is a significant difference in atomic number between the components making up the framework, as under these circumstances the framework distribution can be readily determined using laboratory X-ray diffraction. We are only aware of one study, on $Sr_8Ga_{16}Ge_{30}$,[25] where there was little difference in atomic number, and hence size, between the framework components. Neutrons were used for this work as they provide approximately 10% scattering contrast between the gallium and germanium. However, neutron diffraction is not a universally applicable method for this kind of experiment; absorption and lack of scattering contrast can be problems. Resonant X-ray scattering[27−30] offers an alternative that is applicable for all elements with atomic numbers greater than ∼22 (Ti). In many cases it can provide considerably more scattering contrast than neutron diffraction. Additionally, the scattering contrast can be readily varied by the acquisition of diffraction data at different wavelengths. The use of several data sets with differing scattering contrast reduces the correlations between atomic displacement parameters and occupancies and aids the accurate determination of site occupancies.

In this paper we report the preparation and transport properties (resistivity, Seebeck coefficient, and thermal conductivity) of the new tin clathrate $Cs_8Cd_4Sn_{42}$ along with the results from a careful resonant diffraction study of the material at room temperature. The 20 K structure is also reported. The use of diffraction data collected at three different scattering contrast levels (close to both the Sn and Cd K-edges and at 80.725 keV, Au K-edge) enabled the determination of cadmium and tin site occupancies without any constraints on overall composition or site occupancies. This provides information on both the cadmium distribution and the possible presence of vacancies in the framework.

Experimental Section

Sample Preparation. High-purity elements were mixed in an argon atmosphere glovebox inside a tungsten crucible, which was itself sealed inside a stainless steel canister. The canister was then placed in a furnace at 550 °C for 2 weeks. It was air-quenched to room temperature. The resulting material consisted of small shiny crystals. For transport measurements, the compound was ground to fine powder and then hot pressed inside a graphite die at 380 °C and approximately 2×10^4 lb/in.^{2} for 2 h in an argon atmosphere. The resulting pellet was slowly cooled to room temperature. It had a density of 5.2 g/cm^3 (90% of theoretical). Electron beam microprobe analysis of the polished surface revealed the stoichiometry to be $Cs_8Cd_{3.9}Sn_{42.7}$, normalizing to the Cs content, while no other phases were observed.

Transport Measurements. A parallelpiped piece ($2 \times 2 \times 5$ mm^3) was cut from a hot pressed pellet using a wire saw. Four-probe electrical resistivity (ρ), steady-state Seebeck coefficient (S), and steady-state thermal conductivity (κ) measurements were performed in a radiation-shielded vacuum probe with the heat flow measured along the longest axis. Heat

(21) Kroner, R.; Peters, K.; von Schnering, H. G. *Z. Kristallogr.—New Cryst. Struct.* **1998**, *213*, 669−670.
(22) von Schnering, H. G.; Carrillo-Cabrera, W.; Kroner, R.; Peters, E.-M.; Peters, K. *Z. Kristallogr.—New Cryst. Struct.* **1998**, *213*, 679.
(23) Kroner, R.; Peters, K.; von Schnering, H. G. *Z. Kristallogr.—New Cryst. Struct.* **1998**, *213*, 667−668.
(24) Kroner, R.; Peters, K.; von Schnering, H. G. *Z. Kristallogr.—New Cryst. Struct.* **1998**, *213*, 675−676.
(25) Chakoumakos, B. C.; Sales, B. C.; Mandrus, D. G.; Nolas, G. S. *J. Alloys Compd.* **2000**, *296*, 80−86.
(26) Blake, N. P.; Mollnitz, L.; Kresse, G.; Metiu, H. *J. Chem. Phys.* **1999**, *111*, 3133−3144.
(27) Hodeau, J.-L.; Favre-Nicolin, V.; Bos, S.; Renevier, H.; Lorenzo, E.; Berar, J.-F. *Chem. Rev.* **2001**, *101*, 1843−1867.
(28) Cox, D. E.; Wilkinson, A. P. In *Resonant Anomalous X-ray Scattering: Theory and Applications*; Materlik, G., Sparks, C. J., Fischer, K., Eds.; North-Holland: Amsterdam, 1994; pp 195−219.
(29) Warner, J. K.; Wilkinson, A. P.; Cheetham, A. K. *J. Phys. Chem. Solids* **1991**, *52*, 1251−1256.
(30) Cheetham, A. K.; Wilkinson, A. P. *Angew. Chem., Int. Ed. Engl.* **1992**, *31*, 1557−1570.

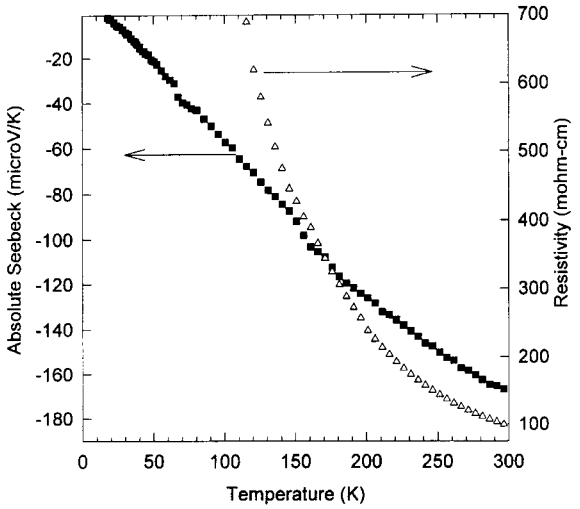

Figure 2. Temperature dependence of the Seebeck coefficient (filled squares) and resistivity (open triangles) for $Cs_8Cd_4Sn_{42}$. The measurements were performed on polycrystalline hot pressed pellets.

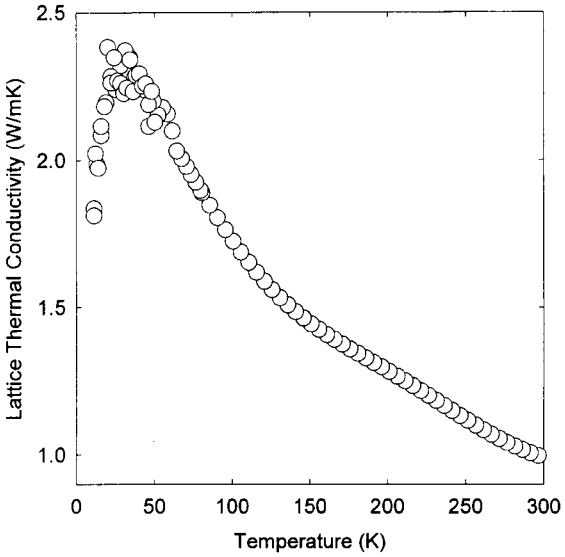

Figure 3. Temperature dependence of the lattice thermal conductivity for $Cs_8Cd_4Sn_{42}$. The measurements were performed on polycrystalline hot pressed pellets.

losses via conduction through the lead wires and radiation were determined in separate experiments, and the data were corrected accordingly. These corrections were approximately 15% at room temperature and less than 5% below 120 K. The temperature dependence of the electronic conductivity and the Seebeck coefficient are shown in Figure 2, and the thermal conductivity is plotted in Figure 3.

X-ray Measurements. Data were acquired using beam line 1-ID of SRI-CAT at the Advanced Photon Source. Room temperature diffraction patterns were acquired at three different photon energies, 80.725 keV (Au K-edge, calibrated wavelength 0.153 659 Å), 29.194 keV (just below the Sn K-edge), and 26.708 keV (just below the Cd K-edge). A 1 mm diameter capillary sample of $Cs_8Cd_4Sn_{42}$ was employed in each case. A recently developed bent double crystal Si(111) Laue monochromator[31] was used for the 80.725 keV measurements, and a Si(311) double crystal Bragg monochromator was used at the lower energies. Additional low-temperature data (20 K) were acquired at 26.708 keV. All the data sets were obtained using a Si(111) analyzer crystal and an Oxford Cyberstar detector. Transmission absorption spectra were recorded at both the Sn and Cd K-edges from a thin sample of $Cs_8Cd_4Sn_{42}$ supported on tape.

Table 1. Details of the Diffraction Data Collection and Analysis

	298 K, 80 keV	298 K, Cd K	298 K, Sn K	20 K, Cd K
wavelength/Å	0.153659	0.464134(2)	0.424666(3)	0.4641344
μ/cm^{-1}	18.5	54	80	54
estimated μR	0.14	0.39	0.60	0.39
trans max/min	0.77/0.77	0.516/0.512	0.373/0.371	0.516/0.512
data range (2θ°)	1.5−12.8	3.8−40.0	3.8−33.0	3.8−50.0
d_{min}/Å	0.69	0.68	0.75	0.55
R_F^2	6.35	6.99	9.95	3.1
R_{wp}	14.84	13.14	16.81	11.25
χ^2	1.742[a]	1.742[a]	1.742[a]	1.732
Cd f'	−0.143	−8.7	−1.64	−8.7
Cd f''	0.563	1.30	3.101	1.30
Sn f'	−0.172	−2.22	−8.5	−2.22
Sn f''	0.659	0.66	1.0	0.66
Cs f'	−0.29	−1.42	−1.68	−1.42
Cs f''	0.948	1.00	0.846	1.00

[a] Value is for the overall refinement including three data sets.

X-ray Data Analyses. Rietveld analyses[32] of the diffraction data were performed using the program GSAS.[33] For the room temperature diffraction data, a single refinement including all three data sets was performed. Resonant scattering factors for the Cs, Sn, and Cd were obtained using a combination of the program FPRIME[34] and Kramers−Kronig transformation based on the measured absorption spectra. The program Chooch[35] was used for the Kramers−Kronig transformation of the Sn K-edge absorption data. As the Cd K-edge absorption data were noisy, resonant scattering factors for the cadmium close to the Cd K-edge were estimated on the assumption that the functional forms of $f'(E)$ and $f''(E)$ for cadmium at the Cd K-edge would be similar to those for tin at the Sn K-edge. During the Rietveld analysis of the room temperature data, it was assumed that the two Cs sites were completely occupied. However, no restraints or constraints were placed on the cadmium and tin contents of the material, and the framework site occupancies were not constrained to sum up to one. This later measure allows for the possibility of vacancies on the framework sites. The 20 K data analysis was performed using a fixed Cd/Sn distribution derived from the analysis of the room temperature resonant scattering data. A trace of β-tin impurity (∼2 wt %) was modeled as a second phase in both refinements. No absorption correction was applied to any of the data, as the relatively short wavelengths used for all the experiments lead to very little variation in sample transmission over the full angular range of the data sets (see Table 1). General details of the refinements are given in Table 1, profile plots are shown in Figure 4, the coordinates and temperature factors are given in Table 2, and bond distances and angles are shown in Table 3.

Results and Discussion

Crystal Structure. The crystal structure consists of face sharing dodecahedral and tetrakaidecahedral cages (see Figure 1a). As has been previously observed for materials of this type, the atomic displacement parameter (ADP) for the atom in the tetrakaidecaheral cavity (Cs(2)) is much larger than that for the atom (Cs(1)) in the dodecahedral cavity (see Table 2). This is attributed

(31) Shastri, S. D.; Mashayekhi, A.; Fezzaa, K.; Lee, W.-K.; Fernandez, P. B.; Tajiri, G. C.; Ferguson, D. A.; Lee, P. L. *APS Activity Report*; Argonne National Laboratory report ANL-00/5: 2001; Vol. 1, pp 258−259.

(32) Rietveld, H. M. *J. Appl. Crystallogr.* **1969**, *2*, 65−71.

(33) Larson, A. C.; Von Dreele, R. B. *GSAS−General Structure Analysis System*; Los Alamos Laboratory Report LA-UR-86-748, 1987.

(34) Cromer, D. T. *J. Appl. Crystallogr.* **1983**, *16*, 437.

(35) Evans, G.; Pettifer, R. F. *J. Appl. Crystallogr.* **2000**, *34*, 82−86.

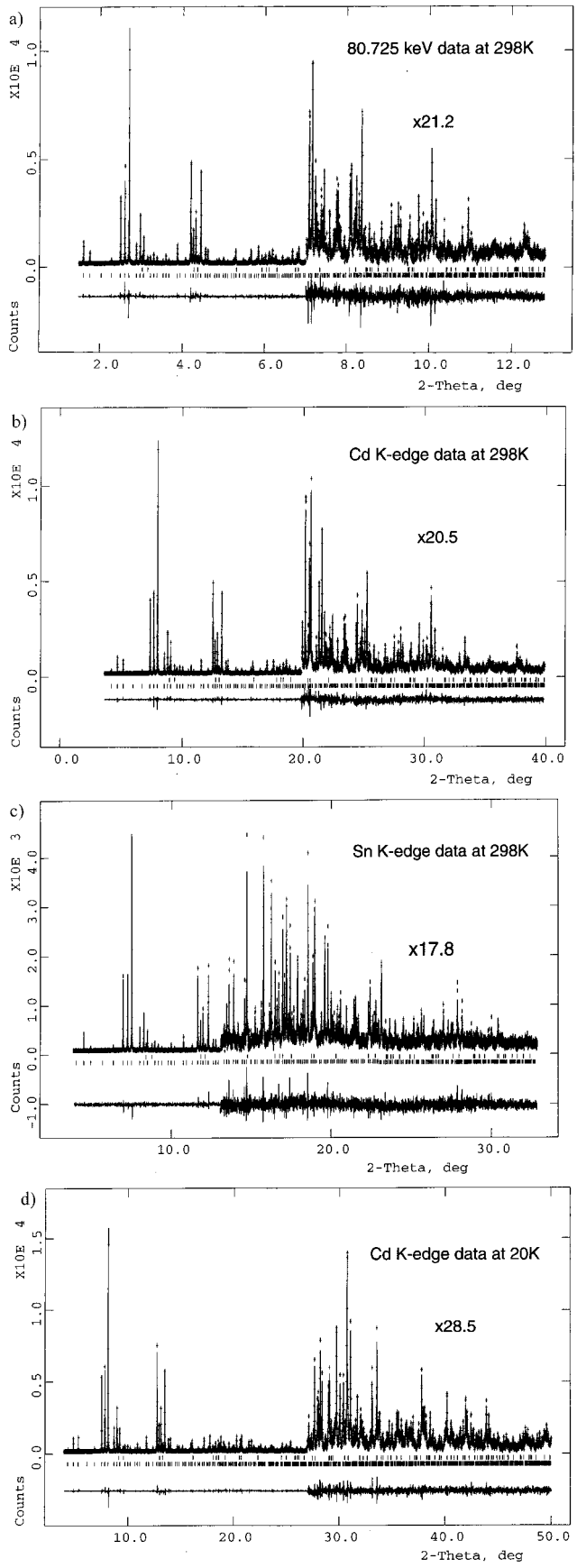

Figure 4. Rietveld profile plots showing fits to the (a) 80.725 keV, (b) Cd K-edge and (c) Sn K-edge data collected at 298 K, and (d) the data collected at 20 K. The crosses are the observed data points, and the solid line is the calculated pattern. The tick marks below the profile indicate the expected peak positions for the $Cs_8Cd_4Sn_{42}$ and the β-tin impurity.

Table 2. Structural Parameters for $Cs_8Cd_4Sn_{42}$ at 298 and 20 K

	298 K	20 K
lattice constant *a*/Å	12.23570(8)	12.20280(3)
Cs(1) U_{iso}/Å^2	0.0130(5)	0.0004(2)
Cs(2) U_{iso}[a]/Å^2	0.0410(5)	0.0080
Sn/Cd(1) U_{iso}/Å^2	0.0117(4)	0.0002(2)
Sn/Cd(1) occup	0.41(2)/0.58(2)	0.33/0.66
Sn/Cd(2) U_{iso}/Å^2	0.0111(2)	0.0007(1)
Sn/Cd(2) occup	1.02(1)/−0.02(1)	1/0
Sn/Cd(2) *x*	0.18306(4)	0.18313(3)
Sn/Cd(3) U_{iso}/Å^2	0.0115(2)	0.00083(8)
Sn/Cd(3) occup	1.00(1)/0.01(1)	1/0
Sn/Cd(3) *y*	0.31037(5)	0.31046(4)
Sn/Cd(3) *z*	0.11750(5)	0.11755(4)

[a] Value from 20 K refinement is U_{eq} as anisotropic ADPs were refined for Cs(2).

Table 3. Bond Lengths (Å) and Angles (deg) for $Cs_8Cd_4Sn_{42}$ at 20 and 298 K

	20 K	298 K
Cs(1)−Sn(2) 8×	3.8706(6)	3.8795(5)
Cs(1)−Sn(3) 12×	4.0509(5)	4.0606(6)
Cs(2)−Sn(1) 4×	4.31434(1)	4.32598(3)
Cs(2)−Sn(2) 8×	4.5400(2)	4.5527(2)
Cs(2)−Sn(3) 8×	4.0883(3)	4.0997(4)
Cs(2)−Sn(3) 4×	4.7249(5)	4.7382(6)
Sn(1)−Sn(3) 4×	2.8217(5)	2.8306(6)
Sn(2)−Sn(2) 1×	2.827(1)	2.838(2)
Sn(2)−Sn(3) 3×	2.8370(4)	2.8437(4)
Sn(3)−Sn(1) 1×	2.8217(5)	2.8306(6)
Sn(3)−Sn(2) 2×	2.8370(4)	2.8437(4)
Sn(3)−Sn(3) 1×	2.869(1)	2.875(1)
Sn(3)−Sn(1)−Sn(3) 4×	109.15(1)	109.15(1)
Sn(3)−Sn(1)−Sn(3) 2×	110.11(2)	110.11(2)
Sn(2)−Sn(2)−Sn(3) 3×	107.54(2)	107.54(2)
Sn(3)−Sn(2)−Sn(3) 3×	111.33(1)	111.33(2)
Sn(1)−Sn(3)−Sn(2) 2×	106.70(2)	106.71(2)
Sn(1)−Sn(3)−Sn(3) 1×	124.95(1)	124.94(1)
Sn(2)−Sn(3)−Sn(2) 1×	103.94(2)	103.93(3)
Sn(2)−Sn(3)−Sn(3) 2×	106.39(1)	106.39(2)

to the "rattling" of Cs(2) in the larger tetrakaidecahedral cavity. Our room temperature ADPs for the Cs atoms are almost identical to those reported for $Cs_8Zn_4Sn_{42}$,[15] and those for the framework atoms are a little smaller than those observed for the zinc compound. The slightly larger cavity size in the cadmium-containing material (1% larger cell constant) does not lead to an obvious increase in the Cs ADPs. The ADPs of clathrates, filled Skutterudites, and similar materials have previously been used by Sales et al. to estimate Einstein temperatures for the "rattling" atoms in these materials, the velocity of sound in the materials, and thermal conductivities.[36,37] Using the approach of Sales et al.,[36,37] our data indicate Einstein temperatures of 91 and 51 K for Cs(1) and Cs(2), respectively (rattling frequencies of 63 and 35 cm^{-1}, respectively), a Debye temperature of 179 K for the framework, and a velocity of sound of 2.05 × 10^3 m s^{-1}. At room temperature the heat capacity is estimated to be close to the classical Dulong and Petit value of 24.9 J K^{-1} per mole of atoms.[38] Assuming that all of the Cs atoms are involved in scattering the phonons responsible for heat transport, the average

(36) Sales, B. C.; Chakoumakos, B. C.; Mandrus, D. *J. Solid State Chem.* **1999**, *146*, 528−532.
(37) Sales, B. C.; Mandrus, D. G.; Chakoumakos, B. C. In *Recent Trends in Thermoelectric Materials Research II*; Tritt, T. M., Eds.; Academic Press: San Diego, 2001; Vol. 70, pp 1−36.
(38) Kittel, C. *Introduction to Solid State Physics*, 6th ed.; John Wiley: New York, 1986.

separation between scattering centers is 6.1 Å, leading to an estimated room temperature thermal conductivity of 0.5 W m^{-1} K^{-1}. If we assume that only the "rattling" Cs(2) atoms are involved in phonon scattering, the average separation between scatters becomes ~6.7 Å, and the thermal conductivity is expected to be ~10% larger. The predicted thermal conductivities are ~50% of the experimentally determined value (Figure 3) and in line with estimates for related materials such as $Sr_8Ga_{16}Ge_{30}$.[36,37]

In the type I clathrates $Sr_8Ga_{16}Ge_{30}$[25] and $Eu_8Ga_{16}Ge_{30}$,[12,39,40] the very large ADPs associated with the atoms in the tetrakaidecahedral cavities are possibly due to static disorder associated with the presence of multiple minima in the potential function for the cavity. However, in $Cs_8Cd_4Sn_{42}$, there is no indication of any static disorder in the tetrakaidecahedral cavities. The ADP for Cs(2) at 20 K is significantly larger than that for Cs(1), but the use of a split site model for Cs(2) does not produce a significantly better fit to the 20 K diffraction data. There are no physically unusual changes in bond lengths on cooling from 298 to 20 K. The decrease of the Sn−Sn bond lengths on cooling is consistent with the thermal expansion coefficient of the material (9.7×10^{-6}/K between 20 and 298 K).

The significant size difference between cadmium and zinc (covalent radii for Cd, Zn, and Sn are 141, 125, and 140 ppm, respectively)[41] is presumably responsible for the larger cell constant for the cadmium-containing material, as compared to $Cs_8Zn_4Sn_{42}$, and it has some effect on the bond lengths. The Sn(1)−Sn(3) bond length is 3% larger for the cadmium-containing material than that reported for the zinc compound, but all of the other Sn−Sn distances are within 1% of the values determined for the zinc compound. The bond angles around the framework sites in the zinc- and cadmium-containing compounds are similar, but the cadmium compound is closer to regular tetrahedral coordination. The observed bond length differences are in line with the covalent radii for Cd, Zn, and Sn; the average bond length around the M(1) site should be ~3.7% less for the zinc-containing compound as the zinc is located entirely on this (6c Wykoff position) site.

Our resonant scattering measurements for the cadmium compound (see Table 2) indicate that the cadmium occupies the 6c site. We allowed for the possibility of cadmium, tin, and vacancies on each framework site during the data analysis. There is no evidence for the presence of any vacancies in the framework (all sites refine to within 1% of fully occupied), and the cadmium was found to be entirely on the 6c site (<2% on other sites). The sample composition obtained from the refinement ($Cs_8Cd_{3.4}Sn_{42.8}$) was very close to that expected for a Zintl compound[14] ($Cs_8Cd_4Sn_{42}$), lending confidence to the overall quality of the resonant scattering data analysis. The X-ray refinement is also in good agreement with the microprobe results ($Cs_8Cd_{3.9}Sn_{42.7}$). The observation that the cadmium goes preferentially to the 6c site is in line with what has been reported for compounds such as $K_8Al_8Sn_{38}$,[24] $Cs_8Ga_8Sn_{38}$,[18] and $Cs_8Zn_4Sn_{42}$[15] where the substituting species differs in size from the major framework component. This indicates that size is not the dominant factor in determining which sites the substituting elements are located on in this family of materials.

It has been reported that the preference of a substituting element or vacancy can be rationalized using the rule of topological charge stabilization[42] along with a Mulliken population analysis;[43] the framework site with the greatest Mulliken population will be substituted by more electronegative species, and electropositive species will go to the site with the lowest Mulliken population. Calculations on the type I clathrate K_8Si_{44} indicate that the 6c site has the lowest Mulliken population of the three crystallographically distinct framework sites in this material.[43] As cadmium is less electronegative than tin ($\chi_{Sn} = 1.96$, $\chi_{Cd} = 1.69$), by analogy with the work on K_8Si_{44}, we would predict the preferential location of cadmium on the 6c site. Electronegativity arguments have previously been employed to rationalize the observed site preferences of antimony in a type I clathrate.[44]

Transport Properties. Figure 2 shows the resistivity (ρ) and Seebeck coefficient (S) as a function of temperature for the polycrystalline $Cs_8Cd_4Sn_{42}$ sample over the range 5−300 K. The negative sign for S indicates that the majority carriers are electrons and the temperature dependence of the resistivity is indicative of semiconducting behavior. From the measured values of ρ and the Wiedemann−Franz law (with ideal Lorenz number, $L_0 = 2.44 \times 10^{-8}$ V^2/deg^2) we can estimate the electronic component of the thermal conductivity, $\kappa_e = L_0T/\rho$. This indicates that κ_e is less than 8% of κ at room temperature. In Figure 3 we display the lattice thermal conductivity, κ_g ($\kappa_g = \kappa - \kappa_e$), of polycrystalline $Cs_8Cd_4Sn_{42}$ over the temperature range 10−300 K. At room temperature, $\kappa_g \sim 1$ W m^{-1} K^{-1}. The κ_g values are relatively low for a crystalline solid and particularly interesting for thermoelectric applications. κ_g increases slowly with decreasing temperature. This is an indication that phonon scattering other than from anharmonic interactions is present in this compound. The localized vibrations, or "rattling", of Cs(2) in $Cs_8Cd_4Sn_{42}$ apparently create strong phonon scattering centers, as indicated by the large ADPs of Cs(2).

Conclusions

The relatively low thermal conductivity of $Cs_8Cd_4Sn_{42}$ is associated with the rattling of cesium in the tetrakaidecahedral cavities of the clathrate structure. There is no evidence for static disorder of the species in the cavities such as that seen in clathrates that display glass like thermal conductivities ($Sr_8Ga_{16}Ge_{30}$ and $Eu_8Ga_{16}Ge_{30}$). Resonant scattering combined with the analysis of multiple data sets collected at different scattering

(39) Sales, B. C.; Chakoumakos, B. C.; Jin, R.; Thompson, J. R.; Mandrus, D. *Phys. Rev. B* **2001**, *63*, 245113-1 to 245113-8.
(40) Chakoumakos, B. C.; Sales, B. C.; Mandrus, D. G. *J. Alloys Compd.* **2001**, *322*, 127−134.
(41) Emsley, J. *The Elements*; Clarendon Press: Oxford, 1991.
(42) Gimarc, B. M. *J. Am. Chem. Soc.* **1983**, *105*, 1979−1984.
(43) Miller, G. J. In *Chemistry, Structure, and Bonding of Zintl Phases and Ions*; Kauzlarich, S. M., Eds.; VCH: New York, 1996; pp 1−59.
(44) Latturner, S.; Bu, X.; Blake, N.; Metiu, H.; Stucky, G. D. *J. Solid State Chem.* **2000**, *151*, 61−64.

contrast levels provides a powerful means for determining the distribution of atoms or vacancies doped into the framework. This approach is in many cases superior to the use of neutron diffraction. $Cs_8Cd_4Sn_{42}$ would absorb neutrons strongly, and laboratory X-rays provide little contrast between cadmium and tin. The resonant scattering data indicated that all the cadmium is present on only one of three inequivalent framework sites and that there are no vacancies in the framework.

Acknowledgment. A.P.W. is grateful for financial support from the NSF under Grant DMR9623890. G.S.N. acknowledges support from the U.S. Army Research Laboratory under Contract DAAD17-99-C-0006 and Marlow Industries. The work at the Advanced Photon Source was supported by the U.S. Department of Energy under Contract W-31-109-Eng-38.

CM0107880